Copyright 2007 Society of Photo-Optical Instrumentation Engineers (SPIE). This paper was published at the SPIE conference Infrared Technology and Applications XXXIII, 2007 in Orlando, USA and is made available as an electronic reprint with permission of SPIE. One print or electronic copy may be made for personal use only. Systematic or multiple reproduction, distribution to multiple locations via electronic or other means , duplication of any material in this paper for a fee or for commercial purposes, or modification of the content of the paper are prohibited.

Uncooled Infrared Bolometer Arrays Operating in a Low to Medium Vacuum Atmosphere: Performance Model and Tradeoffs

Frank Niklaus [*a c], Christer Jansson [c], Adit Decharat [a], Jan-Erik Källhammer [b], Håkan Pettersson [b], Göran Stemme [a]

[a] Microsystem Technology Group, KTH-Royal Institute of Technology, 10044 Stockholm, Sweden

[b] Autoliv Research AB, 447 83 Vårgårda, Sweden

[c] FAUN AB, 18361 Täby, Sweden

Abstract

In this paper we present a comprehensive calculational model for the noise equivalent temperature difference (NETD) of infrared imaging systems based on uncooled bolometer arrays. The NETD model is validated and benchmarked using published performance data of state-of-the-art uncooled infrared bolometer arrays. The calculational model is used to evaluate possible infrared sensor and system design tradeoffs that allow optimization for low-cost infrared systems with improved reliability and lifetime, while still achieving a NETD of about 150 mK, required for pedestrian injury mitigation systems. We propose an approach in which high performance crystalline semiconductor materials with very low 1/f-noise properties and a temperature coefficient of resistance (TCR) of 3 %/K are used as thermistor material for the bolometers. The resulting increased bolometer performance can be used to operate the infrared imaging arrays in a vacuum atmosphere with increased gas pressure while still achieving useful NETD levels. The proposed calculational model suggests that a NETD on the order of 150 mK can be reached with uncooled infrared bolometer arrays operating in vacuum pressures on the order of 6 mbar. Such specifications for the bolometer vacuum package dramatically simplify wafer-level vacuum packaging and ease long-term reliability issues, contributing to lowering the vacuum packaging and thus, the overall infrared imaging chip costs.

Keywords: infrared bolometer array, calculation performance model, noise equivalent temperature difference, NETD

Introduction

Since the early nineties, the interest in uncooled infrared (IR) bolometer arrays has drastically increased. With a dramatic price reduction of uncooled infrared imaging arrays, a growing number of commercial infrared imaging applications will emerge, such as e.g. night vision for automotive applications and infrared imaging based person detection [1, 2]. Various authors have developed figures of merit describing infrared detector or infrared system performances such as responsivity ($\Re$), noise equivalent power (NEP), detecitivity (D*), and noise equivalent temperature difference (NETD) [3-7]. The noise equivalent temperature difference (NETD) is one of the most important performance parameter of an infrared imaging system and is defined as the difference in temperature between two side-by-side blackbodies of large lateral extent which, when viewed by the infrared imaging system, gives rise to a difference in signal-to-noise-ratio of 1 in the electrical outputs of the two halves of the array, viewing the two blackbodies. Uncooled infrared systems can today reach NETDs of as low as 25 mK with a F-number F = 1 of the infrared optics [8-11]. For most commercial infrared imaging applications the required NETD is between 80 mK and 200 mK [1, 2]. Authors have calculated the fundamental performance limits of uncooled infrared bolometers with the NETD limited by the noise from the background radiation and radiation emitted from the bolometer [3, 4, 7]. One group has published an analysis of the detailed noise contributions to the total NETD of bolometers made of vanadium oxide [9]. In this paper, we present a calculational model for the NETD of bolometer based infrared imaging systems, including the relevant noise contributions. The NETD model is benchmarked with

[*] *E-mail: frank.niklaus@ee.kth.se , Tel: +46 (0) 76 216 73 49 , Fax: +46 (0) 8 10 08 58*

published values of existing state-of-the-art infrared bolometer arrays [9, 10]. The model is used to analyze bolometer design features and trade-offs that can improve the performance of uncooled infrared bolometer arrays and reduce the requirements and thus, the costs for the vacuum packaging. A finite element model is used to estimate the thermal conduction between the bolometers and their surrounding when the bolometers are operated in a vacuum atmosphere with increased gas pressure.

Calculational model for the noise equivalent temperature difference (NETD) of infrared bolometer arrays

For conventional uncooled infrared bolometer arrays with a column based read-out design and integrated analogue-to-digital conversion (ADC), the NETD including the contributing NETD parts can be expressed by

$$NETD^2 = NETD_{\frac{1}{f}}{}^2 + NETD_{Johnson}{}^2 + NETD_{thermal}{}^2 + NETD_{ROIC}{}^2 \qquad (Eq.1)$$

where the total NETD consists of the $NETD_{1/f}$ from the 1/f-noise of the bolometer, the $NETD_{Johnson}$ from the Johnson noise of the bolometer, the $NETD_{thermal}$ from the thermal fluctuation noise of the bolometer including noise from radiation heat exchange and the $NETD_{ROIC}$ from the read-out integrated circuit (ROIC) related noise. The contributing NETD parts can be expressed by equations 2 to 10

$$NETD_{\frac{1}{f}} = \left(4 \cdot \frac{F^2}{\phi_{\lambda 1-\lambda 2} \cdot \left(\frac{\Delta P}{\Delta T} \right)_{\lambda 1-\lambda 2}} \right) \cdot \frac{G \cdot \sqrt{\frac{K}{\upsilon}} \cdot \sqrt{\ln\left(\frac{f_r}{f_s} \right)} \cdot \sqrt{1 + \omega^2 \cdot \left(\frac{C}{G} \right)^2}}{TCR \cdot \beta \cdot A \cdot \varepsilon_{\lambda 1-\lambda 2}} \qquad (Eq.2)$$

$$NETD_{Johnson} = \left(4 \cdot \frac{F^2}{\phi_{\lambda 1-\lambda 2} \cdot \left(\frac{\Delta P}{\Delta T} \right)_{\lambda 1-\lambda 2}} \right) \cdot 2 \cdot \sqrt{k} \cdot \frac{G \cdot \sqrt{R_{bol}} \cdot \sqrt{f_r} \cdot \sqrt{T_1} \cdot \sqrt{1 + \omega^2 \cdot \left(\frac{C}{G} \right)^2}}{U_{bias} \cdot TCR \cdot \beta \cdot A \cdot \varepsilon_{\lambda 1-\lambda 2}} \qquad (Eq.3)$$

$$NETD_{thermal} = \left(4 \cdot \frac{F^2}{\phi_{\lambda 1-\lambda 2} \cdot \left(\frac{\Delta P}{\Delta T} \right)_{\lambda 1-\lambda 2}} \right) \cdot 4 \cdot \sqrt{k} \cdot \frac{f_{eff} \cdot T_1 \cdot \sqrt{C}}{\beta \cdot A \cdot \varepsilon_{\lambda 1-\lambda 2}} \qquad (Eq.4)$$

$$NETD_{ROIC} = \left(4 \cdot \frac{F^2}{\phi_{\lambda 1-\lambda 2} \cdot \left(\frac{\Delta P}{\Delta T} \right)_{\lambda 1-\lambda 2}} \right) \cdot \frac{(R_{ROIC} + R_{bol}) \cdot G \cdot \sqrt{1 + \omega^2 \cdot \left(\frac{C}{G} \right)^2}}{R_{ROIC} \cdot U_{bias} \cdot TCR \cdot \beta \cdot A \cdot \varepsilon_{\lambda 1-\lambda 2}} \cdot V_{ROIC} \qquad (Eq.5)$$

$$V_{ROIC} = \sqrt{V_{amp}(f_r)^2 + \frac{V_Q^2}{12} + \left(\frac{R_{ROIC} \cdot R_{bol}}{R_{ROIC} + R_{bol}} \right)^2 \cdot I_{ROIC}(f_r)^2} \qquad (Eq.6)$$

Copyright 2007 Society of Photo-Optical Instrumentation Engineers (SPIE).

$$f_r = x_l \cdot f_i \qquad \textit{(Eq.7)}$$

$$f_{eff} = \min\left| f_r , f_{bol} \right| \qquad \textit{(Eq.8)}$$

$$f_{bol} = \frac{1}{4 \cdot \tau} \qquad \textit{(Eq.9)}$$

$$\tau = \frac{C}{G} \qquad \textit{(Eq.10)}$$

where F is the F-number of the infrared optics, $\phi_{\lambda 1-\lambda 2}$ is the transmission of the infrared optics in the wavelength interval from λ1 to λ2, G is the total thermal conduction between the bolometer and its surrounding, C is the thermal capacity of the bolometer pixel, TCR is the temperature coefficient of resistance of the thermistor material (temperature sensing bolometer material), K is the 1/f noise constant of the thermistor material, υ is the volume of the thermistor material, R_{bol} is the resistance of the bolometer thermistor (bolometer resistance), β is the bolometer fill factor, A is the bolometer pixel area (pixel pitch), $\varepsilon_{\lambda 1-\lambda 2}$ is the infrared absorption rate of the bolometer membrane in the wavelength interval from λ1 to λ2, f_s is the shutter or uniformity correction frequency for the bolometer array, f_r is the read-out frequency of the bolometer, x_l is the amount of bolometer pixels per column (number of bolometers that are read-out during one imaging frame), f_i is the image read-out frequency (imaging frame rate), f_{eff} is the effective integration frequency of the bolometer, f_{bol} is the thermal integration frequency of the bolometer, τ is the thermal time constant of the bolometer pixel, U_{bias} is the bolometer bias voltage, R_{ROIC} is the input impedance of the ROIC, V_{ROIC} is the total noise voltage of the ROIC, V_{amp} is the input reference noise voltage of the ROIC (depending on the ROIC architecture, a function of f_r), V_Q is the input reference analogue-to-digital quantization interval, I_{ROIC} is the current noise from the ROIC input including the bolometer bias current source (depending on the ROIC architecture, a function of f_r), $\left(\frac{\Delta P}{\Delta T}\right)_{\lambda 1-\lambda 2}$ is the temperature contrast in the wavelength interval from λ1 to λ2, T_1 is the bolometer membrane temperature, ω is the modulation frequency of the infrared signal from the image scene and k is the Boltzmann constant. The effective integration frequency f_{eff} of the bolometer equals either the read-out frequency f_r or the thermal integration frequency f_{bol} of the bolometer, depending on which of the two is smaller as depicted in equation 8. For conventional bolometer arrays with a large amount of bolometer pixels per column and a low thermal conduction between the bolometers and their surrounding, the effective integration frequency f_{eff} of a bolometer typically equals the thermal integration frequency f_{bol} of the bolometer. Equations 1 to 10 are valid for the assumption that the difference between the bolometer temperature and the surrounding temperature is small [3].

Figure 1 shows schematic cross-sectional views of two typical infrared bolometer designs containing resonant optical cavity structures to achieve a high absorption rate $\varepsilon_{\lambda 1-\lambda 2}$ of the incident infrared radiation. In the resonant optical cavity design shown in Figure 1a, the resonant optical cavity is part of the bolometer membrane. The mirror of this type of resonant optical cavity is placed at the lower surface of the bolometer membrane and the thickness of the bolometer membrane defines the optical cavity. The membrane thickness is typically set to $\frac{\lambda_x}{4}$, where λ_x is the wavelength of the targeted infrared radiation in the bolometer membrane material(s) [17]. Bolometers with resonant optical cavities as shown in Figure 1a are emitting

Copyright 2007 Society of Photo-Optical Instrumentation Engineers (SPIE).

infrared radiation both from the upper and lower surfaces of the bolometer membranes. At the same time incoming (background) infrared radiation is absorbed only from the upper surface of the bolometer membrane while incoming (background) infrared radiation to the lower surface of the bolometer membrane is reflected by the mirror layer. In the resonant optical cavity design shown in Figure 1b, the mirror of the resonant optical cavity is placed on the surface of the underlying substrate (the ROIC) and the bolometer membrane is placed at a distance of $\frac{\lambda}{4}$ from the mirror surface on the substrate. Thus, a high fraction of the incident infrared radiation at a specific wavelength λ is absorbed in the bolometer membrane [9]. For a targeted wavelength interval of 8 μm to 14 μm, the distance between the bolometer membrane and the mirror on the substrate is typically about 2 μm to 2.5 μm [9, 12]. In such a bolometer design only the upper surface of the bolometer membrane is effectively radiating. Infrared radiation that is emitted from the lower surface of the bolometer membrane is reflected by the mirror on the substrate and absorbed again by the bolometer membrane. At the same time, incoming (background) infrared radiation is absorbed both from the upper and the lower surfaces of the bolometer membrane.

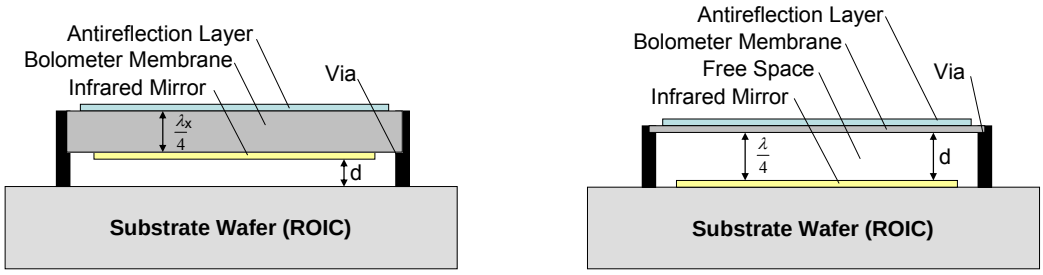

(a) (b)

Figure 1: *Cross-sectional image of two bolometer designs with resonant optical cavities for high absorption of the incident infrared radiation.*

The thermal capacity of the bolometer pixel can be expressed by [12]

$$C = V_1 \cdot \rho_1 \cdot c_1 + V_2 \cdot \rho_2 \cdot c_2 + \ldots \qquad \textit{(Eq.11)}$$

where V_x is the volume of each bolometer membrane material, ρ_x is the density of each bolometer membrane material and c_x is the mass specific heat of each bolometer membrane material. The total thermal conduction between a bolometer and its surrounding can be estimated by [12]

$$G = G_{\text{leg-conduction}} + G_{\text{radiation}} + G_{\text{gas-conduction}} + G_{\text{convection}} \qquad \textit{(Eq.12)}$$

where $G_{\text{leg-conduction}}$ is the thermal conduction between the bolometer and its surrounding through the bolometer legs, $G_{\text{radiation}}$ is the thermal conduction between the bolometer and its surrounding by emitted heat radiation, $G_{\text{gas-conduction}}$ is the thermal conduction between the bolometer and its surrounding through the gas, and $G_{\text{convection}}$ is the thermal conduction between the bolometer and its surrounding by gas convection. The thermal conduction $G_{\text{leg-conduction}}$ through bolometer legs consisting of several material layers (e.g. a structural dielectric layer and a metal layer for the electrical contacts between the bolometer and the ROIC) can be expressed by [12]

$$G_{leg-conduction} = 2 \cdot \left(\lambda_{leg-material1} \cdot \frac{A_{leg-material1}}{l_{leg}} + \lambda_{leg-material2} \cdot \frac{A_{leg-material2}}{l_{leg}} + \ldots \right) \qquad \textit{(Eq.13)}$$

Copyright 2007 Society of Photo-Optical Instrumentation Engineers (SPIE).

where $\lambda_{leg\text{-}materialx}$ is the thermal conductivity of each bolometer leg material, $A_{leg\text{-}materialx}$ is the cross sectional area of each bolometer leg material, and l_{leg} is the length of the bolometer legs [12]. With the assumptions that the temperature difference between the bolometer membrane and its surrounding is small, the thermal conduction $G_{radiation}$ by emitted infrared radiation can be expressed as [12, 13]

$$G_{radiation} = 8 \cdot \sigma \cdot \delta \cdot \beta \cdot A \cdot T_1^3 \qquad \textit{(Eq.14)}$$

where σ is the Stefan-Boltzmann constant, δ is the effective emissivity of the bolometer membrane, β is the bolometer fill factor, A is the bolometer pixel area (pixel pitch), and T_1 is the temperature of the bolometer membrane [12]. Equation 14 is valid for bolometer designs as shown in Figure 1a, in which both the upper and the lower surfaces of the bolometer membranes are emitting infrared radiation. If bolometer designs as shown in Figure 1b are used, in which effectively only the upper surfaces of the bolometer membranes are emitting infrared radiation, equation 14 has to be divided with a factor of 2 [12, 15]. In most practical cases the thermal conduction $G_{radiation}$ by emitted infrared radiation is negligible compared to the thermal conduction $G_{leg\text{-}conduction}$ through the bolometer legs [12].

If a bolometer array is operated in a vacuum atmosphere, both the thermal conduction $G_{gas\text{-}conduction}$ through the gas and the thermal conduction $G_{convection}$ by gas convection is negligible [12, 13]. In this situation, the thermal conduction between the bolometer and its surrounding is dominated by the thermal conduction $G_{leg\text{-}conduction}$ through the bolometer legs. If a bolometer array is operated in a gas atmosphere, the thermal conduction $G_{gas\text{-}conduction}$ through the gas contributes significantly to the total thermal conduction G between the bolometer and its surrounding. For practical cases, the thermal conduction $G_{convection}$ by gas convection is negligible compared to the thermal conduction $G_{gas\text{-}conduction}$ through the gas [12, 13]. With the assumption that the distance d between the lower bolometer surface and the substrate is small (on the order of 2-3 μm) compared to the distance between the upper bolometer surface and the infrared window of the bolometer array package and that the thermal conduction between the bolometer membrane and the neighbouring bolometer pixels is negligible, the thermal conduction $G_{gas\text{-}conduction}$ through the surrounding gas can be expressed by [12, 14]

$$G_{gas-conduction} = \lambda_{gas-p} \cdot \frac{\beta \cdot A}{d} \qquad \textit{(Eq.15)}$$

where $\lambda_{gas\text{-}p}$ is the thermal conductivity of the gas at a fixed gas pressure p and d is the distance between bolometer membrane and the substrate. The thermal conductivity of the gas in dependence of the gas pressure p and the distance d between the bolometer membrane and the substrate can be expressed by [12, 14]

$$\lambda_{gas-p}(p,d) = \frac{1}{\frac{1}{\lambda_{gas}} + \frac{1}{\gamma_{gas} \cdot p \cdot d}} \qquad \textit{(Eq.16)}$$

where p is the pressure of the gas, λ_{gas} is the pressure-independent thermal conductivity of the gas in the high-pressure regime ($\lambda_{air} = 0.024 \ \frac{W}{K \cdot m}$ for air), and γ_{gas} is the thermal conductivity per unit pressure and length in the low-pressure regime ($\gamma_{air} = 1.9 \ \frac{m}{K \cdot s}$ for air) [12]. If the distance between the bolometer membrane and the substrate is large (on the order of 10-20 μm) and the distance to the neighbouring

Copyright 2007 Society of Photo-Optical Instrumentation Engineers (SPIE).

bolometer pixels is small (on the order of 1-2 μm), the thermal conduction between the bolometer and the neighbouring bolometer pixels is not negligible [14]. For such bolometer membranes, a finite element simulation will provide a better estimate of the resulting thermal conduction between the bolometer and its surrounding than equations 15 and 16. Equations 1 to 10 of the NETD model are derived from equations 17 to 25, which are commonly used equations [3-7] modified to take the influence of the ROIC input impedance into account

$$NETD = \frac{4 \cdot F^2 \cdot V_N}{\Re \cdot A \cdot \phi_{\lambda 1-\lambda 2} \cdot \left(\frac{\Delta P}{\Delta T} \right)_{\lambda 1-\lambda 2}} \qquad \textit{(Eq.17)}$$

$$\Re = \frac{TCR \cdot \beta \cdot \varepsilon_{\lambda 1-\lambda 2} \cdot R_{eff} \cdot I_{bias}}{G \cdot \sqrt{1+\omega^2 \tau^2}} \qquad \textit{(Eq.18)}$$

$$V_N{}^2 = V_{\frac{1}{f}}{}^2 + V_{johnson}{}^2 + V_{thermal}{}^2 + V_{ROIC}{}^2 \qquad \textit{(Eq.19)}$$

$$V_{\frac{1}{f}} = R_{bol} \cdot I_{bias} \cdot \sqrt{\frac{K}{\upsilon}} \cdot \sqrt{\ln\left(\frac{f_r}{f_s} \right)} \cdot \frac{R_{ROIC}}{R_{ROIC} + R_{bol}} \qquad \textit{(Eq20)}$$

$$V_{johnson} = 2 \cdot \sqrt{k} \cdot \sqrt{T_1 \cdot R_{bol} \cdot f_r} \cdot \frac{R_{ROIC}}{R_{ROIC} + R_{bol}} \qquad \textit{(Eq.21)}$$

$$V_{thermal} = 2 \cdot \sqrt{k} \cdot \frac{\Re \cdot T_1 \cdot \sqrt{G \cdot f_{eff}}}{\beta \cdot \varepsilon_{\lambda 1-\lambda 2}} \qquad \textit{(Eq.22)}$$

$$V_{ROIC} = \sqrt{V_{amp}^2 + V_{ADC}^2 + R_{eff}^2 \cdot I_{ROIC}^2} \qquad \textit{(Eq.23)}$$

$$V_{ADC} = \frac{V_Q}{\sqrt{12}} \qquad \textit{(Eq.24)}$$

$$R_{eff} = \frac{R_{bol} \cdot R_{ROIC}}{R_{bol} + R_{ROIC}} \qquad \textit{(Eq.25)}$$

where $\Re$ is the responsivity, R_{eff} is the resulting resistance of the parallel bolometer resistance and the ROIC input impedance, I_{bias} is the bias current of the bolometer, V_N is the total noise voltage of infrared imaging system, , $V_{1/f}$ is the 1/f-noise voltage, $V_{Johnson}$ is the Johnson noise voltage, $V_{thermal}$ is the thermal fluctuation noise voltage including the radiation noise voltage, V_{ROIC} is the total read-out integrated circuit noise voltage for a column parallel read-out structure with integrated AD conversion and V_{ADC} is the noise voltage of the analogue-to-digital converter.

Copyright 2007 Society of Photo-Optical Instrumentation Engineers (SPIE).

Benchmarking of the NETD model

The NETD model described by equations 1 to 16 was validated and benchmarked using published values for the contributing NETD parts from a state-of-the-art uncooled infrared bolometer array operated in a vacuum [9, 10]. This array consists of 640 x 480 bolometer pixels made of vanadium oxide (VO_x) with a pixel pitch of 28 µm x 28 µm. The VO_x bolometers contain optical cavity structures as shown in Figure 1b and thus, equation 14 has to be divided with a factor of 2 [12, 15] when estimating the total thermal conductance G between a bolometer and its surrounding. Figure 2 shows a close-up view of the infrared bolometer array [9].

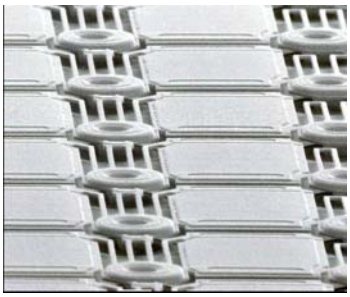

Figure 2: *Vanadium oxide (VO_x) bolometer array with a pixel pitch of 28 µm x 28 µm [9].*

The published total system NETD for this uncooled infrared bolometer array is 29 mK with the published contributing NETD parts being [9]

$$(NETD)^2 = (NETD_{\frac{1}{f}})^2 + (NETD_{Johnson})^2 + (NETD_{thermal})^2 + (NETD_{ROIC})^2$$

$$\| \qquad \| \qquad \| \qquad \| \qquad \|$$

$$(29\text{ mK})^2 = (25.5\text{ mK})^2 + (8.5\text{ mK})^2 + (6.5\text{ mK})^2 + (9.5\text{ mK})^2$$

The NETD model described by equations 1 to 16 correctly predicts these contributing NETD parts when the bolometer and system design parameters are set to the values shown in Table 1. All values in Table 1 are typical values for the respective parameters used in uncooled infrared bolometer arrays [3-11, 16].

Optimization of bolometer design features and tradeoffs

For many of the above mentioned applications, array sizes on the order of 80 x 30 pixels and system NETDs on the order of 150 mK are sufficient [1, 2]. Equations 1 to 16 show that a number of design parameters are available to optimize infrared imaging systems based on uncooled bolometer arrays for reduce requirements on the gas pressure in the vacuum package and thus, for low-cost and improved reliability. The design parameters that show promise for improving the resulting NETD of an infrared bolometer array with a given bolometer pixel pitch, are the 1/f noise constant K, the volume of the bolometer thermistor material υ, the total thermal conduction G between the bolometer and its surrounding, the temperature coefficient of resistance TCR of the bolometer thermistor material, the fill factor β of the bolometer, the infrared absorption rate $\varepsilon_{\lambda 1-\lambda 2}$ of the bolometer membrane, the bolometer bias voltage U_{bias} and the ROIC noise voltage V_{ROIC}.

The design parameters in Table 1 together with equations 1 to 16 show that the NETD of state-of-the-art uncooled infrared bolometer arrays is dominated by the 1/f noise related $NETD_{1/f}$ part. Equation 2 shows that the $NETD_{1/f}$ part can be very efficiently decreased by decreasing the 1/f-noise constant K of the bolometer thermistor material. The 1/f noise constant K is a thermistor material parameter that can vary several orders

Copyright 2007 Society of Photo-Optical Instrumentation Engineers (SPIE).

Table 1: *Bolometer and infrared system parameters used to validate the NETD model.*

Parameters:	**Parameter values [3, 9, 10]:**		
Boltzmann constant	k =	$1.38 \cdot 10^{-23}$	$\frac{J}{K}$
Stefan-Boltzmann constant	σ =	$5.67 \cdot 10^{-8}$	$\frac{J}{(K^4 \cdot m^2 \cdot s)}$
Temperature contrast in the wavelength interval from 8 µm to 14 µm at a temperature of 300 K	$\left(\frac{\Delta P}{\Delta T}\right)_{8-14\,\mu m}$ =	2.624	$\frac{W}{(K \cdot m^2)}$
F-number of the infrared optics	F =	1	-
Total thermal conduction between the bolometer and its surrounding when operated in a vacuum atmosphere	G =	$3.7 \cdot 10^{-8}$	$\frac{W}{K}$
Thermal conductance between the bolometer and its surrounding by emitted infrared radiation	$G_{radiation}$ =	$0.18 \cdot 10^{-8}$	$\frac{W}{K}$
Thermal capacity of the bolometer membrane	C =	$4.34 \cdot 10^{-10}$	$\frac{J}{K}$
Thermal time constant of the bolometer	τ =	$1.17 \cdot 10^{-2}$	s
Bias voltage of the bolometer	U_{bias} =	2	V
Bolometer pixel area (pixel pitch = 28 µm x 28 µm)	A =	$7.84 \cdot 10^{-10}$	m^2
Bolometer fill factor	β =	0.62	-
Pixel count of the bolometer array (columns x lines)	x_c x x_l =	640 x 480	pixels
Image read-out frequency (image frame rate)	f_i =	30	Hz = $\frac{1}{s}$
Parameters:	**Estimated parameter values [4-8, 11, 16]:**		
Transmission of the infrared optics in the wavelength interval from 8 µm to 14 µm	$\phi_{8-14\,\mu m}$ =	0.98	-
Absorption of the bolometer membrane in the wavelength interval from 8 µm to 14 µm	$\varepsilon_{8-14\,\mu m}$ =	0.92	-
Bolometer membrane temperature	T_1 =	298	K
Resistance of the vanadium oxide (VO_x) thermistor material (bolometer resistance)	R_{bol} =	$2.6 \cdot 10^4$	Ω
Temperature coefficient of resistance of the vanadium oxide (VO_x) thermistor material	TCR =	0.02	$\frac{1}{K}$
Thickness of the vanadium oxide (VO_x) thermistor material	h_{VOx} =	$8.0 \cdot 10^{-8}$	m
Volume of the vanadium oxide (VO_x) thermistor material (= $\beta \cdot A \cdot h_{VOx}$)	υ =	$3.89 \cdot 10^{-17}$	m^3
1/f-noise constant of the vanadium oxide (VO_x) thermistor material	K =	$4.0 \cdot 10^{-29}$	m^3
Volume specific 1/f-noise constant of the bolometer	$\frac{K}{\upsilon}$ =	$1.03 \cdot 10^{-12}$	
Effective emissivity of the bolometer membrane	δ =	0.6	
Input impedance of the ROIC (ROIC resistance)	R_{ROIC} =	$2.6 \cdot 10^4$	Ω
Current noise from the ROIC input including the bolometer bias current source	I_{ROIC} =	$8.0 \cdot 10^{-11}$	A
Input referred ADC quantization interval	V_Q =	$2 \cdot 10^{-6}$	V
Input referred noise voltage of the ROIC	V_{amp} =	$0.8 \cdot 10^{-6}$	V
Total noise voltage of the ROIC	V_{ROIC} =	$1.4 \cdot 10^{-6}$	V
Shutter / uniformity correction frequency	f_s =	$1.66 \cdot 10^{-2}$	Hz = $\frac{1}{s}$
IR modulation frequency	ω =	30	Hz = $\frac{1}{s}$

Copyright 2007 Society of Photo-Optical Instrumentation Engineers (SPIE).

of magnitude for different materials and even small variations of the material composition can have a dramatic impact on K [7]. For most materials K is not very well documented in literature, however epitaxial grown, mono-crystalline materials can have a much lower K than amorphous or poly-crystalline materials. Thus, the $NETD_{1/f}$ and ultimately the total NETD can be reduced efficiently by applying mono-crystalline thermistor materials [7, 9]. Equations 1 to 16 predict an improved NETD of 17 mK if a high-performance bolometer thermistor material is used with $K = 4.0 \cdot 10^{-30}$ m^3 (a factor of 10 decreased K as compared to the VO_x bolometer thermistor material in Table 1), while leaving all other bolometer design parameters from Table 1 unchanged. However, conventional monolithic integration of the thermistor material on top of a ROIC wafer limits the deposition process for the thermistor material to 450ºC and does not allow the deposition of mono-crystalline materials.

Heterogeneous, three-dimensional (3D) bolometer integration has been proposed for the integration of semiconductor grade mono-crystalline thermistor materials on ROICs [17, 19, 20]. In heterogeneous 3D bolometer integration, the thermistor material is epitaxially grown on a separate handle wafer. The thermistor material is then transferred from the handle wafer to the ROIC wafer using low-temperature adhesive wafer bonding in combination with sacrificial removing of the handle wafer as shown in Figure 3.

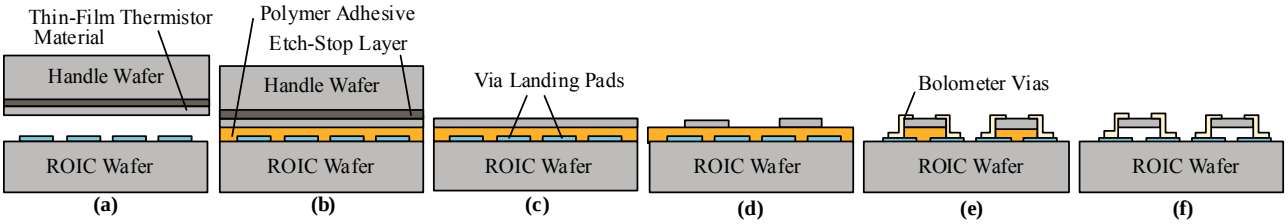

Figure 3: *Heterogeneous 3D integration of uncooled infrared bolometer arrays: (a) separate fabrication of ROIC wafer and handle wafer with bolometer thermistor material (b) adhesive wafer bonding (c) thinning of handle wafer (d) bolometer definition (e) via formation (f) sacrificial etching of the adhesive.*

To provide a low total thermal conduction G between a bolometer and its surrounding, the bolometer legs are long, their cross-sectional area is small and they consist of materials with low thermal conductivities. To achieve a sufficiently low NETD, conventional infrared bolometer arrays are in addition operated in a vacuum atmosphere to minimize the thermal conduction between the bolometer and its surrounding through the gas. For the total thermal conduction G between a typical bolometer design and its surrounding to be entirely dominated by the thermal conduction through the bolometer legs, the vacuum atmosphere in which the bolometer is operated is on the order of 0.01 mbar [18]. To lower packaging cost for infrared bolometer arrays and improve the reliability of the package, infrared bolometer arrays may be operated in a vacuum atmosphere with increased gas pressure. However, in such a situation, the thermal conduction $G_{gas\text{-}conduction}$ between the bolometers and their surrounding through the gas increases significantly, which results in a significantly increased NETD.

Infrared bolometer arrays operating in a vacuum atmosphere with increased gas pressure

A three-dimensional thermal finite element bolometer model has been developed to determine the total thermal conduction G between the bolometer and its surrounding in dependence of the gas pressure p and the distance d between the bolometer membrane and the substrate surface. For the finite element model, the Comsol Multiphysices™ software was used. Figure 4a shows the thermal circuit model for a bolometer, where G_{leg} is thermal conduction between the bolometer and the substrate through the bolometer legs, G_{gap_memb} is the thermal conduction between the bolometer and the substrate through the gas that is surrounding the bolometer and G_{gap_lat} is thermal conduction between the bolometer and the neighbouring

Copyright 2007 Society of Photo-Optical Instrumentation Engineers (SPIE).

bolometer pixels through the gas. The thermal conduction between the bolometer and the infrared window (or lens) through the gas, the thermal conduction between the bolometer and its surrounding by gas convection and the thermal conduction between the bolometer and its surrounding by emitted infrared radiation are negligible and not included in this finite element model. The resulting total thermal conduction between the bolometer and its surrounding G_{eq} is the combination of the parallel and series connected thermal conduction paths. In the finite element simulation, the total thermal conduction G_{eq} between the bolometer and its surrounding is determined by calculating the heat flow rate between the bolometer membrane and the heat sink (substrate) and divide it with the temperature difference between the bolometer membrane and the heat sink (substrate). Figure 4b shows the heat flow paths between the bolometer membrane and a substrate connection (SC) through the bolometer legs and through the surrounding gas.

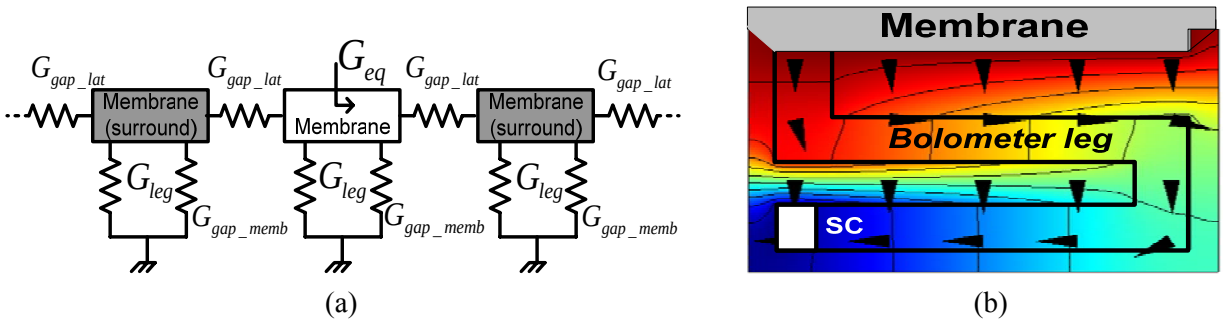

(a) (b)

Figure 4: *(a) Thermal circuit model for the bolometer and (b) top view of a bolometer leg with parts of the bolometer membrane and a substrate connection (SC) including the heat flow paths.*

In the finite element model, the bolometer dimensions are selected to be similar to the dimensions of the bolometer shown in Figure 2, with the bolometer membrane 18 µm x 27 µm in size. The bolometer legs are 32 µm long, 1 µm wide and defined as a sandwich of 0.1 µm thick silicon nitride and 0.015 µm thick titanium. The thickness of the bolometer membrane is set to 1.5 µm and the gap distances to the neighbouring bolometer membranes are set to 2 µm. For the simulations, the thermal conductivity of air at different pressures $\lambda_{air\text{-}p}$ has been calculated according to equation 16. Figure 5(a) shows a graph of the thermal conductivity of air $\lambda_{air\text{-}p}$ in dependence of the gas pressure p for distances d between the bolometer membrane and the substrate of 3 µm, 7 µm and 12 µm. The thermal conductivities used for the calculations are $\lambda_{Ti} = 21.9 \frac{W}{K \cdot m}$ for titanium, $\lambda_{SiN} = 3.2 \frac{W}{K \cdot m}$ for silicon nitride, $\lambda_{air} = 0.024 \frac{W}{K \cdot m}$ for air and $\gamma_{air} = 1.9 \frac{m}{K \cdot s}$ for air. Figure 5b shows a graph of the simulated total thermal conduction G_{eq} between a bolometer and its surrounding in dependence of the gas pressure p for distances d between the bolometer membrane and the substrate surface of 3 µm, 7 µm and 12 µm.

The design parameters of an 80 x 30 pixels infrared bolometer array have been optimized for operation in a vacuum atmosphere with increased gas pressure. Therefore the use of a heterogeneously integrated, high-performance mono-crystalline bolometer thermistor material is assumed. The design parameters from Table 1 have been optimized to x_c x x_l = 80 x 30 pixels, $\frac{K}{\upsilon} = 1.03 \cdot 10^{-13}$ (with a factor of 10 decreased $\frac{K}{\upsilon}$ as compared to the VO_x bolometer thermistor material in Table 1), TCR = 0.03 $\frac{1}{K}$, $V_{ROIC} = 10^{-6}$ V,

Copyright 2007 Society of Photo-Optical Instrumentation Engineers (SPIE).

C =2.43·10^{-9} $\frac{J}{K}$ (with a total bolometer membrane thickness of 1.5 µm), while leaving all other parameters in Table 1 unchanged. Figure 5c shows a graph of the calculated NETD of the proposed infrared bolometer array in dependence of the gas pressure p for distances d between the bolometer membrane and the substrate of 3 µm, 7 µm and 12 µm. From Figure 5c it can be seen that a system NETD of about 150 mK seems possible with bolometers operating in a package containing a gas pressure on the order of 6 mbar. For the proposed design parameters, a gas pressure of 6 mbar and a distance d between the bolometer membranes and the substrate of 3 µm, the NETD is expressed by

$$(NETD)^2 = (NETD_{\frac{1}{f}})^2 + (NETD_{Johnson})^2 + (NETD_{thermal})^2 + (NETD_{ROIC})^2$$

$$\| \qquad \| \qquad \| \qquad \| \qquad \|$$

$$(152\ \text{mK})^2 = (98\ \text{mK})^2 + (29\ \text{mK})^2 + (62\ \text{mK})^2 + (93\ \text{mK})^2$$

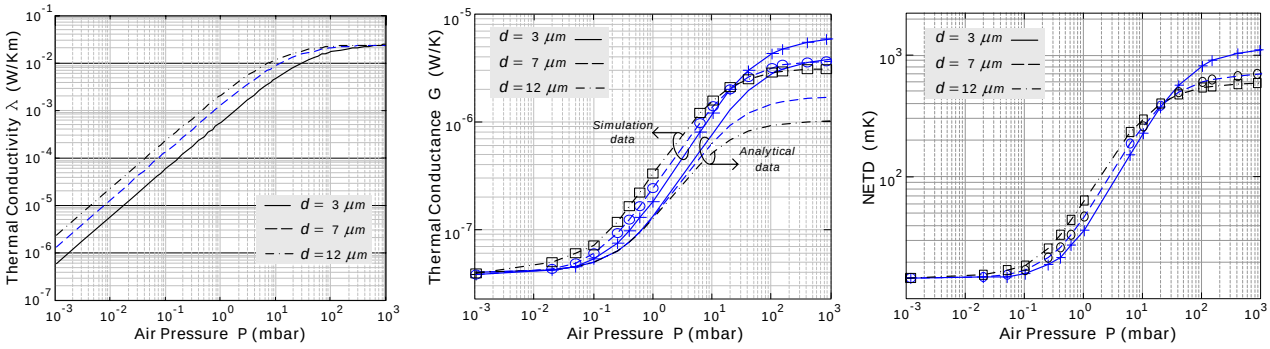

Figure 5: *(a) thermal conductivity of the air in dependence of the gas pressure, (b) simulated total thermal conduction between a bolometer and its surrounding in dependence of the gas pressure and (c) calculated bolometer system NETD in dependence of the gas pressure.*

For bolometers operated in a vacuum atmosphere with increased gas pressure, a bolometer design as shown in Figure 1a is more suitable than the design shown in Figure 1b since it provides the possibility for the comparably high thermal mass C of the bolometer membrane and a variable distance d between the bolometer membrane and the substrate. For bolometers operated in a vacuum atmosphere with a very low gas pressure, a bolometer design as shown in Figure 1b is more suitable and can reach lower absolute NETD values. This is due to the fact that a very low total thermal conductance G between the bolometers and their surrounding can be used in combination with a very low thermal mass C of the bolometer membranes.

Conclusions

The proposed calculational model makes it possible to estimate the resulting NETD of infrared imaging systems based on uncooled bolometer arrays. The model is validated using published NETD data from a state-of-the-art infrared bolometer array that is based on state-of-the-art vanadium oxide (VO_x) bolometers. The proposed NETD model allows the optimization of the design parameters of infrared bolometer systems. The calculation results suggest that bolometer thermistor materials with low 1/f-noise can achieve a useful NETD on the order of 150 mK when operated in a vacuum atmosphere with a gas pressure on the order of 6 mbar.

Acknowledgements

The authors gratefully acknowledge support from the Swedish IVSS program and from Vinnova.

Copyright 2007 Society of Photo-Optical Instrumentation Engineers (SPIE).

References

[1] M. Hirota, Y. Nakajima, M. Saito, M. Uchiyama, "Thermoelectric infrared imaging sensors for automotive applications", *Proc SPIE 2004*, Vol. 5359, pp. 111-125, San Jose, USA.

[2] J.-E. Källhammer, H. Pettersson, D. Eriksson, S. Junique, S. Savage, C. Vieider, J.Y. Andersson, F. Niklaus, G. Stemme, "Fulfilling the pedestrian protection directive using a long-wavelength infrared camera designed to meet the performance and cost targets", *Proc. SPIE 2006*, Vol.6198, pp.74-84, Strasbourg, France.

[3] P.L. Marasco, E.L. Dereniak, "Uncooled infrared sensor performance", *Proc. SPIE 1993*, Vol. 2020, pp. 363-378, San Diego, USA.

[4] P.W. Kruse, "*Uncooled thermal imaging arrays, systems and applications*", SPIE Press, Bellingham, WA, USA, 2001.

[5] R.A. Wood, "Uncooled mocrobolometer infrared sensor arrays", in *Infrared Emitters and Detectors*, edited by P. Capper, C.T. Elliott, Kluwer Academic Publishers, Norwell, Massachusetts, 2001.

[6] V.Y. Zerov, V.G. Malyarov, I.A. Khrebtov, "Calculational modeling of the main characteristics of an uncooled linear microbolometer array", *Journal of Optical Technology*, Vol. 7, No. 3, pp. 153-157, 2004.

[7] P.W. Kruse, "Can the 300 K radiating background noise limit be attained by uncooled thermal imagers ?", *Proc. SPIE 2004*, Vol. 5406, pp.437-446, Orlando, USA.

[8] E. Mottin, A. Bain, J.L. Martin, J.L. Ouvrier-Buffet, S. Bisotto, J.J. Yon, J.L. Tissot, "Uncooled amorphous silicon technology enhancement for 25 μm pixel pitch achievement", *Proc. SPIE 2003,* Vol. 4820, pp. 200-207, Seattle, USA.

[9] M. Kohin, N. Buttler, "Performance limits of uncooled VOx microbolometer focal plane arrays", *Proc. SPIE 2004*, Vol. 5406, pp.447-453, Orlando, USA.

[10] B. Backer, M. Kohin, A. Leary, R. Blackwell, R. Rumbaugh, "Advances in uncooled technology at BAE systems", *Proc. SPIE 2003*, pp. 548-556, Orlando, USA.

[11] D. Murphy, M. Ray, J. Wyles, J. Asbrock, C. Hewitt, R. Wyles, E. Gordon, T. Sessler, A. Kennedy, S. Baur, D. Van Lue, "Performance improvements for VOx microbolometer FPAs", *Proc. SPIE 2004*, pp. 531-540, Orlando, USA.

[12] P. Eriksson, J.Y. Andersson, G. Stemme, "Thermal characterization of surface-micromachined silicon nitride membranes for thermal infrared detectors", *IEEE Journal of Microelectromechanical Systems*, Vol. 6, No. 1, pp. 55-61, 1997.

[13] J.J. Talghader, "Thermal and mechanical phenomena in micromechanical optics", *Journal of Physics D: Applied Physics*, Vol. 37, pp. R109-R122, 2004.

[14] X. He, G. Karunasiri, T. Mei, W.J. Zeng, P. Neuzil, U. Sridhar, "Performance of microbolometer focal plane arrays under varying pressure", *IEEE Electron Device Letters*, Vol. 21, No. 5, pp. 233-235, 2000.

[15] S. Tohyama, M. Miyoshi, S. Kurashina, N. Ito, T. Sasaki, A. Ajisawa, N. Oda, "New thermally isolated pixel structure for high-resolution uncooled infrared FPAs", *Proc. SPIE 2004*, Vol. 5406, pp.428-436, Orlando, USA.

[16] C. Jansson, U. Ringh, K. Liddiard, N. Robinson, "FOA/DSTO uncooled IRFPA development", *Proc. SPIE 1999*, Vol. 3698, pp. 264-275, Orlando, USA.

[17] F. Niklaus, J. Pejnefors, M. Dainese, M. Haggblad, P.-E. Hellström, U.J. Wallgren, G. Stemme, "Characterization of transfer-bonded silicon bolometer arrays", *Proc. SPIE 2004*, Vol. 5406, pp. 521-530, Orlando, USA.

[18] J.J. Yon, L. Biancardini, J.L. Tissot, L. Letellier, "Infrared microbolometer sensors and their application in automotive safety", *Proc. AMAA 2003,* pp.1-15, Berlin, Germany.

[19] F. Niklaus, E. Kälvesten, G. Stemme, "Wafer-level membrane transfer bonding of polycrystalline silicon bolometers for use in infrared focal plane arrays", *Journal of Micromechanics and Microengineering*, Vol. 11, pp. 509-513, 2001.

[20] F. Niklaus, G. Stemme, J.-Q. Lu, R.J. Gutmann, "Adhesive wafer bonding", *Journal of Applied Physics, Applied Physics Reviews - Focused Review*, Vol. 99, No. 3, pp. 031101/1-031101/28, 2006.

Copyright 2007 Society of Photo-Optical Instrumentation Engineers (SPIE).